Pitkänen, M.; Kaikkonen, Ossi; Koskelainen, Ari

In vivo monitoring of mouse retinal temperature by ERG photoresponses

Published in:
Experimental Eye Research

DOI:
10.1016/j.exer.2019.05.015

Published: 01/10/2019

Document Version
Peer-reviewed accepted author manuscript, also known as Final accepted manuscript or Post-print

Accepted Manuscript

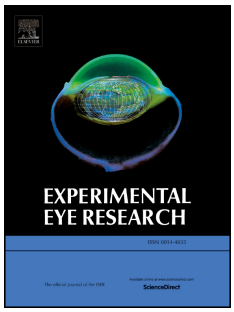

In vivo monitoring of mouse retinal temperature by ERG photoresponses

Marja Pitkänen, Ossi Kaikkonen, Ari Koskelainen

PII: S0014-4835(19)30205-2

DOI: https://doi.org/10.1016/j.exer.2019.05.015

Reference: YEXER 7675

To appear in: *Experimental Eye Research*

Received Date: 4 April 2019

Revised Date: 14 May 2019

Accepted Date: 21 May 2019

Please cite this article as: Pitkänen, M., Kaikkonen, O., Koskelainen, A., *In vivo* monitoring of mouse retinal temperature by ERG photoresponses, *Experimental Eye Research* (2019), doi: https://doi.org/10.1016/j.exer.2019.05.015.

In vivo monitoring of mouse retinal temperature by ERG photoresponses

Marja Pitkänen, Ossi Kaikkonen, and Ari Koskelainen

Department of Neuroscience and Biomedical Engineering, Aalto University School of Science, P.O. Box 12200, 00076 Aalto, Finland

Corresponding author: Prof. Ari Koskelainen, email: ari.koskelainen@aalto.fi, tel: +358 50 367 3768, P.O. Box 12200, 00076 Aalto, Finland

Declaration of interest: Pitkänen, none; Kaikkonen, none; Koskelainen, patent application.

ABSTRACT

Non-damaging heating of the retina and RPE provides a promising treatment for retinal diseases. However, the lack of proper control over the temperature hinders the development of safe and repeatable procedures. Here, we demonstrate with mice a non-invasive method for estimating the temperature changes in the retina and the RPE during a heating procedure. The method is based on monitoring the temperature dependent properties of retinal photoresponses recorded by electroretinography (ERG).

In this study, our aim was to investigate the feasibility of ERG signal for retinal temperature estimation, utilizing a-wave and b-wave kinetics as the source of temperature information. We quantified the temperature dependencies of photoresponse kinetics and developed two linear regression models between the temperature and the photoresponse features, enabling temperature estimation. With the first model, based on the a-wave of a single photoresponse, the RMS error obtained for retinal temperature estimation was < 0.9 ℃. The second model, applying the b-waves of five dim flash responses, an RMS error of < 0.7 ℃ was achieved. In addition, we tested the sensitivity of the method to small changes in light stimulus strength and investigated suitable stimulus intervals for continuous retinal temperature monitoring.

The proposed method provides a convenient technique for monitoring mouse retinal and RPE temperature with ERG recording when studying controlled retinal heating. Similar temperature dependencies exist in human ERG suggesting that this approach could also be applicable in clinical heating treatments.

Keywords: Retina, Electroretinography, Retinal pigment epithelium, Heating treatment, Temperature, Kinetics

Abbreviations

ERG	electroretinography
RPE	retinal pigment epithelium
RMS(D)	root mean square (deviation)
BIC	Bayesian information criterion

FIR	finite impulse response
PID	proportional-integral-derivative

1. INTRODUCTION

The retina is a layered tissue at the bottom of the eye responsible for transducing the information carried by light into neural signals. Retinal temperature can be elevated by directing intense light to the fundus, where the pigments of the retinal pigment epithelium (RPE) and the choroid act as main absorbers. Photocoagulation is an established treatment procedure that applies strong retinal heating leading to a visible damage in the treated area. In recent years, researchers have shown increasing interest in developing novel retinal heating treatments that aim at avoiding the damage in retinal cells. The retinal disorders to be addressed include e.g. age-related macular degeneration, central serous chorioretinopathy, diabetic macular edema, and retinal vein occlusion (Lavinsky et al., 2016; Luttrull et al., 2015; Scholz et al., 2017; Sivaprasad et al., 2010; Söderberg et al., 2012; Sramek et al., 2011; Tode et al., 2018). Finding a heating power that is high enough for therapeutic effect but avoids cellular damage is considered as the main challenge in the development of non-damaging heating treatments (Lavinsky et al., 2016; Scholz et al., 2017; Sivaprasad et al., 2010). The amount of temperature elevation in the retina and RPE is dependent e.g. on the fundus pigmentation level and ocular media clarity of each individual as well as the amount of pigmentation and choroidal blood flow at the location of the heated area (Connolly et al., 2003; Ibarra et al., 2004; Parver, 1991). Therefore, applying equivalent heating power for each patient leads to varying levels of temperature rise.

Currently, clinical retinal heating treatments apply either a fixed heating power or a titration method to adjust the heating for each individual. In the titration method, a reference treatment causing a visible lesion is defined in the peripheral retina. A certain proportion of this reference treatment (e.g. lower laser power or duty cycle) is then applied to the desired retinal area (see e.g. Koss et al., 2012; Lavinsky et al., 2016). This method, however, leads to permanent damage in the peripheral area and does not take into account the variation in local pigmentation. In addition, accurate determination

of the visible lesion may be difficult. Thus, a method for retinal temperature monitoring, providing online temperature information directly from the treated area would offer a substantial benefit, improving safety, repeatability, and efficacy of the treatment.

Electroretinography (ERG) is a technique for obtaining information on retinal function by non-invasive recording and it serves as a prominent tool in basic and clinical retinal research. In our previous publication, we introduced a novel idea of applying the temperature dependent properties of ERG photoresponses for the estimation of retinal and/or RPE temperature changes. Furthermore, we provided a proof of concept for this idea by demonstrating temperature determination based on ERG photoresponses with isolated mouse retinas (Pitkänen et al., 2017). However, in order to apply this method in practice, it is necessary to demonstrate its functionality with living animals. In this study, we calibrate the method for mouse corneal ERG flash responses and investigate whether these responses provide information on the retinal temperature changes with sufficient accuracy for retinal heating treatments. The objective is to establish an ERG-based retinal temperature estimation approach for mice *in vivo*.

Retinal responses to flashes of light express acceleration in kinetics with increasing temperature, as the activation and deactivation mechanisms of photoresponses become faster (see Baylor et al., 1983; Lamb, 1984; Robinson et al., 1993 for photoreceptor single cell recordings, Donner et al., 1988; Nymark et al., 2005; Vinberg and Koskelainen, 2010 for photoreceptor ERG, and Kong and Gouras, 2003; Mizota and Adachi-Usami, 2002 for mouse *in vivo* ERG). Studying and quantifying mouse corneal ERG responses as a function of temperature requires the retinal temperature to be manipulated as precisely as possible without invasive procedures affecting the recorded signal. Our solution was to adjust the temperature of the whole body by placing the anesthetized animal in a water bath with precise temperature control while recording the ERG. The determination of temperature dependencies was based on the assumption that, with this setup, mouse retinal temperature coincides with the core body temperature. Both dim and bright light flash stimuli were employed and several features representing the kinetics were extracted from the resulting responses. The features were examined as a function of temperature change and a model enabling temperature

estimation was constructed. The accuracy and generalizability of the model was assessed with a separate set of test data. We also tested the effect of varying the stimulus interval and compared the usage of bright and dim flashes for continuous temperature monitoring. The reliability of our experimental setup was evaluated by comparing the results to those obtained in the previous study (Pitkänen et al., 2017) with isolated retinas.

2. MATERIALS AND METHODS

2.1 Ethical approval

The use and handling of the animals were in accordance with the Finnish Act on Animal Experimentation 2013 and approved by the Animal Experiment Board in Finland (project license ESAVI/6345/04.10.07/2015).

2.2 Mouse anesthesia and ERG recording

2 – 4 month old male and female mice of strain C57BL/6J were maintained on a light dark cycle of 12 h/12 h and dark-adapted overnight before the experiment. Thereafter, all handling was done under a dim red light. The mouse was anesthetized with isoflurane (device: Univentor U-410, AgnTho's AB, Lidingö, Sweden, isoflurane: Virbac group, Carros, France) and placed on a polycarbonate bed equipped with anesthetic supply. The respiration was monitored with a piezoelectric sensor (Pico Movement Sensor, MFi BV, Heerlen, The Netherlands) placed under the mouse and the isoflurane concentration was adjusted to keep the respiratory frequency between 2.0 and 2.5 Hz. Temperature-controlled water circulation under the bed enabled animal's body temperature to be held at ~37.5 ℃ during the prepa rations. The left pupil was dilated by both 10 $mg \cdot ml^{-1}$ atropine sulphate eyedrop (Chauvin Pharmaceuticals Ltd., London, UK) and 100 $mg \cdot ml^{-1}$ phenylephrine HCl eyedrop (Chauvin Pharmaceuticals Ltd., London, UK), and the corneas of both eyes were anesthetized with 4 $mg \cdot ml^{-1}$ oxybuprocaine HCl eyedrops (Santen Ltd., Tampere, Finland). 0.2 mm thick contact lenses were placed on both eyes, a clear acrylic lens on the left eye and an identical black lens on the right eye, which served as a reference. Both lenses were equipped

with a peripherally located acrylic shaft containing a cylindrical Ag-AgCl pellet electrode (EP1, diameter 1 mm, length 3 mm, World Precision Instruments Ltd., Hitchin, UK). Electrical contact between the pellet and cornea as well as moisturization of the cornea was facilitated by methylcellulose solution (5 mg soluted in 1 ml 0.9% NaCl). Instead of the contact lens, a different type of reference electrode setup was used in some experiments. The alternative electrode holder was constructed using a 1ml syringe, whose tip was placed around the reference eye. The syringe was equipped with the Ag-AgCl pellet and filled with the methylcellulose solution to provide electrical contact between the cornea and the pellet. A third Ag-AgCl pellet, moisturized with the methylcellulose solution, was attached to the polycarbonate bed in contact with the mouse's mouth behind the upper incisor teeth. This electrode defined the signal ground. The DC-ERG signals were amplified 1000x, low-pass filtered (eight-pole Bessel filter, f_c = 1 kHz) and digitized at 10 kHz with 30 nV resolution. Light stimuli were generated by two 520 nm laser diodes (LD-520-120MG, 120 mW, Roithner Lasertechnik GmbH, Vienna, Austria), controlled with laser diode controller (iC-HG EVAL HG1D, iC-Haus GmbH, Bodenheim, Germany) driven by computer controlled command pulses. Stimulus strength was adjusted by changing light flash duration between 0.1 µs and 2 ms. These flash lengths are considerably shorter than the integration time of rod photoreceptors, and therefore they can be considered as impulse-like stimuli. Light was guided through a mixing optical cable (Trifurcated fiber bundle, Newport Spectra-Physics GmbH, Darmstadt, Germany) to a cylindrical aluminum stimulator head (inner diameter 5.5 mm, length 2.5 mm), which was placed close to the mouse's head around the left eye. Between the cable and the stimulator head, three diffusor layers were placed to even the intensity profile. Light arrived to the eye both directly across the cylindrical head and by reflecting from the inner walls, illuminating the entire retina. The irradiance of the reflected light was approximately half of the irradiance of the direct light, measured with an optical power meter (PM100D, Thorlabs Sweden AB, Mölndal, Sweden).

2.3 Temperature control and experiment protocol

The mouse resting on its abdomen on the polycarbonate bed was slid inside a rectangular cuboid-shaped water bath tilted at 45° angle and water level was adjusted just below the ears, as shown in Figure 1. The head of the mouse was supported with a polycarbonate plate behind the ears to reduce the occasional movement artefacts caused by mouse breathing or the water flow. Under anesthesia, the ability of the mouse to maintain steady body temperature is compromised, allowing the body temperature to be controlled by changing the temperature of the environment. A peristaltic pump circulated the water in the bath and the body temperature of the animal was adjusted by controlling the temperature of the inflowing water with a custom-made PID-controller connected to a water heating element. The air around the mouse's head was heated to approximately 30 ℃ to decrease tempe rature gradients. The body temperature was monitored using a rectal thermistor (Betatherm 30K6A309I, Oy Farnell Finland Ab, Helsinki, Finland). At steady temperatures, retinal temperature was assumed to coincide with the body temperature. After the preparations under dim red light, the animal was dark-adapted for 15 minutes before any recordings. Light stimulus strengths were selected for each mouse based on their individual operation range of ERG responses at the reference body temperature 37.5 ℃. This approach enables the stimulus strengths to be selected in a similar manner regardless of differences in ERG-recording setups or in the photometric unit used in light stimulus calibration. Additionally, this method takes into account and compensates for the differences in ocular media transparency and photoreceptor sensitivity of each individual. At first, a small set of responses to different stimulus strengths was recorded to map the operation range. A response with a prominent b-wave and a small emerging a-wave (amplitude ~30 – 50 µV) provided the b-wave reference amplitude, 'b-ref-amp', which was used as a measure for adjusting all other stimuli (see Figure 2b). Dim flash responses with an amplitude of 20% of the b-ref-amp were recorded in all 22 experiments. Additionally, in 16 experiments, dim flash responses with amplitudes of 30% and 40% of the b-ref-amp were acquired. Responses to bright stimuli were recorded in 14 experiments. The flash strength used as a bright flash was approximately 1000 times higher than that of the 20% response, inducing a pronounced ~150 – 250 µV a-wave. Responses were first recorded at the reference temperature of

37.5 ℃. Thereafter, the body temperature was adjusted to different values between 35.5 – 42.6 ℃, the approximate rate of temperature change being 0.1 – 0.3 ℃ min^{-1}. After the rectal thermistor reading had reached a steady value, the temperature was let to stabilize for 2 minutes before recordings were performed.

--- Fig 1 ---

2.4 Pre-processing and Feature Extraction

The analysis of the ERG responses was performed in Matlab 2016b, MathWorks. The dataset recorded from 22 mice was split into training (n = 14) and test (n = 8) sets randomly. The test dataset was used only for the validation of the developed model. In the training dataset, 5 – 20 dim flash responses were averaged for the determination of the temperature dependencies (Figure 4 and Table 1) and for the development of the temperature estimation models (Figure 5A-B and 6A-B). The RMS error of the selected model, calculated by cross validation of the training dataset, was based on five averaged responses to estimate the temperature determination accuracy that can be obtained with a certain number of responses. Five dim flash responses were averaged also in the test dataset when investigating the generalizability of the selected model (Figure 5C-D and 6C-D). Bright flash responses were always used without averaging.

A set of temperature-dependent features were extracted from the photoresponses as explained in Appendix. The features correspond to those introduced earlier in (Pitkänen et al., 2017), except for the integration time (#32), which was defined in a slightly different manner and the stretch feature (#12 & #33,) which is a new feature. The feature values of the responses recorded at elevated or lowered temperatures, Y_{temp}, were normalized by the corresponding feature value, Y_{ref}, recorded at reference body temperature 37.5 ℃ 10-40 minutes earlier according to equation $(Y_{temp} - Y_{ref}) \cdot Y_{ref}^{-1}$. As an exception, the normalized value of the stretch feature was calculated by subtracting 1, because the feature already includes a comparison to the reference by definition. The expected value of all normalized features at the reference temperature is zero, and accordingly, the intercepts of linear fits were fixed to 0. All elevated or lowered

temperatures were denoted as differences compared to reference body temperature $T_{temp} - T_{ref}$.

2.5 Model development and validation

Multivariable linear regression models between the temperatures and the normalized feature values were created by least squares fitting of the equation

$$c = X\beta + \varepsilon, \quad (1)$$

where c is the vector of temperatures, X is the matrix of feature values (of training set), β consists of regression coefficients and ε of error terms. A set of candidate models contained all combinations of 1 – 6 features. In model development, adding more features to the model often leads to better fit, but the additional features begin to represent random variation in the data, causing overfitting and weaker generalizability of the model. In order to avoid this, model selection among a set of candidate models can be performed with an information criterion, which introduces a penalty term, increasing as more features are added to the model. In this study, Bayesian information criterion (BIC) was applied, calculated for each model according to the equation

$$BIC = n \cdot \ln\left(\frac{SSE}{n}\right) + k \cdot \ln(n), \quad (2)$$

where n is the number of observations (ERG-response - temperature pairs) in the training dataset, SSE is the sum of squared temperature estimation errors in leave-one-out cross validation of the training dataset, and k is the number of estimated parameters (regression coefficients) in the model. The model with the lowest BIC was selected as the final model. The accuracy of the selected model was evaluated by calculating the errors of temperature determination using the photoresponses of the test dataset.

3. RESULTS

3.1 Mouse corneal ERG flash responses

The retinal temperature determination method developed in this paper is founded on the ERG responses elicited with flash stimuli in scotopic conditions, providing a stable and

well-defined state of the retinal neurons. A set of mouse corneal scotopic ERG responses to varying flash strengths recorded at the reference body temperature is presented in Figure 2A. Responses show the a-wave with negative polarity and the slower positive b-wave. With dim flashes, only the b-wave is visible, peaking at approximately 100 ms after the stimulus. Flash strengths were selected for each mouse based on its individual operation range (amplitude-flash strength behavior) as illustrated in Figure 2B and explained in Methods. Figures 2C and 2D visualize the temperature-related changes in the photoresponses. In Figure 2C, the bright flash response recorded at 1.3 ℃ lower temperature (dashed trace) shows slightly slower kinetics compared to the response evoked by the same stimulus at reference body temperature (solid trace). As the temperature is increased by 3.3 ℃, acceleration of kinetics occurs, as shown in Figure 2D for dim flash responses (solid traces vs. dashed traces). Figures 2C and 2D also illustrate the temperature-dependent features of the responses that will be presented in chapter 3.2.

--- Fig 2 --

In order to test whether the temperature determination method is sensitive to moderate variations in the fractional response amplitude, we recorded dim flash responses with amplitudes 20, 30, and 40% of b-wave reference. For the comparison, we used the time-to-peak feature, whose values are plotted in Figure 3. Linear fittings to the three amplitude groups reveal temperature dependence slopes -0.0365, -0.0360, and -0.0360, respectively. Based on Figure 3, no systematical difference between the feature values or the temperature dependence slopes can be observed. In the remainder of this work, all flash responses with amplitudes in the range 20 – 40% of b-wave reference amplitude are combined for dim flash response analysis and applied in the development of the temperature determination model. Based on this test, the temperature estimation method is expected to be applicable for dim flash responses of moderately varying amplitude.

--- Fig 3 ---

3.2 Temperature dependencies of the features

Thirty-three different temperature-dependent features were extracted from the recorded responses, as illustrated in Figures 2C and 2D. The features were selected to represent the kinetics of the leading edge of the bright flash response a-wave and the entire dim flash response b-wave. The usage of bright flash responses was motivated by the initial phase of the a-wave (before b-wave starts to overlap) originating in the outer segments of photoreceptors partially embedded in the RPE layer. Thus, they could provide the closest approximation of the RPE layer temperature. On the other hand, using dim flash responses would allow higher stimulus repetition frequency and thus better temporal resolution for temperature monitoring (see chapter 3.5). The extracted features are listed in Table 1 and the temperature dependencies of exemplary features are plotted in Figure 4. The behavior of all features as a function of temperature was approximately linear within the temperature range examined. The slopes of linear fits to the data together with the RMS of the residuals are presented in Table 1. The linear fits show about 2.0 – 3.5% change in feature values per 1 ℃ (compared to the value at reference temperature).

--- Table 1 ---

--- Fig 4 ---

3.3 Model development and validation for bright flash responses

Next, we utilized features #1-13 to investigate the applicability of bright flash response a-wave leading edge for retinal temperature estimation. Figure 5A presents the RMS error of temperature determination for single feature regression models. The error is calculated through cross validations of the training dataset. Based on the result, the features determined close to the a-wave peak show highest temperature estimation accuracy. Also time to the inflection point performs well. The temperature determination model was constructed by calculating BIC values for the models consisting of all combinations of 1 – 6 features. Figure 5B displays the lowest BIC value obtained with each number of features. Based on this plot, a model with one feature was selected for further analysis. The model consisted of time-to-peak of the a-wave:

$$Temperature = -27.25 \cdot a100\ (°C)$$

The RMS error of this model at cross-validation with training data was 0.82 ℃. The generalizability of the constructed model was assessed by applying the model to a new set of photoresponses (test dataset) and comparing the resulting temperature estimates to the actual measured temperatures. Each estimate is based on a single bright flash response. Figure 5C illustrates the relationship between estimated and measured temperature, and Figure 5D shows the histogram of error values, giving an RMS error of 0.82 ℃.

--- Fig 5 ---

3.4 Model development and validation for dim flash responses

To study the applicability of dim flash response kinetics for retinal temperature estimation, we constructed and tested regression models with features #13-33, representing the entire response trace. Figure 6A presents the comparison of the performance of single feature regression models in cross validation. Time-to-X% features determined from the leading edge close to the peak, including the time-to-peak feature itself, showed the lowest RMS errors. Based on the behavior of BIC values, illustrated in Figure 6B, a dim flash response model with the following three features was selected: time-to- peak of the b-wave, time-to-60% of b-wave peak (trailing edge), and b-wave stretch:

$$Temperature = -37.66 \cdot b100 + 25.59 \cdot b60T - 13.43 \cdot bst\,(^{\circ}C)$$

The RMS error obtained with the dim flash response model at cross-validation of the training data was 0.68 ℃. The generalization of th e model to test data is illustrated in Figures 6C-D, showing the relationship between the estimated and the measured temperatures and the histogram of temperature estimation errors. Each estimate is based on five averaged dim flash responses. The obtained RMS error for the test data was 0.68 ℃.

--- Fig. 6 ---

3.5 Time interval between flashes

342 The temperature determination method developed in this paper is based on the analysis
343 of dark-adapted (scotopic) flash photoresponses. When applying this kind of method for
344 online temperature determination, the interval between light stimuli should be kept long
345 enough to enable the recovery of photoresponse mechanisms to dark-adapted state
346 between the flashes. Otherwise, light adaptation affects ERG response kinetics (e.g.
347 Friedburg et al., 2001; Nymark et al., 2005) and confounds the temperature
348 determination. We used time-to-peak as a measure to assess whether response
349 mechanisms have recovered, stable time-to-peak indicating long enough stimulus
350 interval. Figure 7A plots b-wave time-to-peak values of four subsequent dim flash
351 responses triggered with 0.5 – 4.3 second interval. With time intervals below 1.3 s
352 (black squares and red circles), response kinetics show clear acceleration characteristic
353 for light adaptation. This behavior is undetectable with longest time intervals (green
354 diamonds and purple stars) implying that 3 - 4 second flash interval is sufficient for
355 recording dark-adapted dim flash responses. In this examination, responses with 40%
356 amplitude of the b-ref-amp were applied to find out a safe interval that is applicable also
357 with weaker stimuli. The sufficient interval for bright flashes was examined by applying a
358 single bright flash to the retina and monitoring the time-to-peak of the following dim flash
359 responses (~10% of b-ref-amp). Figure 7B presents the behavior of time-to-peak after
360 the bright flash and an exponential fitted to averaged data. Based on the result, it takes
361 approximately 20 seconds for the time-to-peak to reach a stable level after a bright
362 flash. The experiments presented in Figure 7 were conducted at 37.5 ℃, indicating that
363 the given intervals are applicable at normal body temperature and at elevated
364 temperatures, where photoresponse recovery mechanisms are accelerated.

365 --- Fig 7 ---

366

367 ## 4. DISCUSSION

368 ### 4.1 Evaluation of sources of error and comparison to *ex vivo* data

369 The temperature determination models developed in this paper were evaluated based
370 on their ability to estimate temperatures both in the training dataset and with a separate

test dataset. In both cases, a single bright flash response could estimate the measured temperature with an RMS error of 0.82 ℃ and averaging five dim flash responses produced an RMS error of 0.68 ℃. These accuracies can be considered good enough to enable the adjustment of desired laser power in RPE heating. In our *ex vivo* setup, RMS errors when using a single bright flash response were 0.56 ℃ in the training dataset and 0.85 ℃ in the test dataset. The corresponding RMS errors for dim flash responses were 0.37 ℃ (training dataset, 8 averaged responses), 0.37 ℃ (test dataset, 8 averaged responses), and 0.40 ℃ (test dataset, 2 averaged responses). The temperature estimation accuracy with *in vivo* ERG can, thus, be considered somewhat inferior to that of *ex vivo* ERG. One reason for slightly weaker accuracy is the lower signal-to-noise ratio of *in vivo* ERG. Another reason may be the time delay associated with the manipulation of mouse body temperature. Changes in the ERG flash response may occur during the time between the recordings at reference temperature and at lowered/elevated temperature due to reasons not directly related to temperature change. This increases the variation in relative feature values *in vivo*. Fortunately, this type of error is not expected in transpupillary heating treatment setup, because the reference ERG responses can be recorded just before the heating with minimal time delay.

Other possible sources of error not covered by the temperature estimation error above include: 1) uncertainty of the retinal temperature in the whole body temperature manipulation method and 2) estimating the RPE temperature based on the temperature of the distal retina. These will be addressed below.

The analysis conducted in this paper is based on the assumption that, with steady temperatures, retinal temperature closely coincides with the core body temperature of the mouse in our experimental setup. This assumption is supported by the following aspects: i) Intensive choroidal circulation, located immediately behind the retina and the monolayer of RPE cells, effectively controls the temperature of the outer retina (Parver, 1991). ii) Majority of the animal is under water creating a constant temperature around the body and enhancing the thermal contact between the body and the environment. iii) The air around mouse's head is heated to reduce the temperature gradient across the

eye. In our recording setup, a small constant difference between the retinal temperature and core body temperature would not be detrimental because the model is linear and temperatures are determined relative to the reference temperature. A difference in the temperature *change* of the core and the retina would, however, affect the calibration of temperature dependencies. In this respect, the present results about the temperature dependencies can be assessed by comparing to our previous data from isolated mouse retinas, for which similar experiments were conducted with precise temperature adjustments (Pitkänen et al., 2017). Dim flash b-wave kinetics features (#13-31 in Table 1) of *in vivo* and *ex vivo* recordings show very similar temperature dependencies. For example, the change in time-to-peak of the b-wave compared to the value at the reference temperature is 3.5% per 1 ℃ for *ex vivo* and 3.6% for *in vivo*. In *ex vivo* conditions, b-wave trailing edge kinetics features have slightly steeper temperature dependence (~3.5% per 1 ℃) than those of the leadi ng edge (~2.5% per 1 ℃). *In vivo*, the temperature dependence of the features representing both edges is 2.7 - 3.2% per 1 ℃, settling between the values obtained *ex vivo*. Bright flash a-wave kinetics features (#1-12) show slightly steeper temperature dependencies *in vivo* compared to *ex vivo*, especially when determined close to the a-wave peak. For example for a-wave time-to-peak, the difference is 1.1 percentage points per °C. This discrepancy is mostly explained by the nonlinear temperature dependence behavior observed in the a-wave kinetics close to the peak *ex vivo*. In highest temperatures tested, the a-wave time-to-peak of the isolated retina did not show as strong acceleration as would be expected based on linear behavior (see Figure S1). When comparing the temperature dependence of the a-wave time-to-peak of *ex vivo* and *in vivo* responses only in the range of -2.0 … +4.5 ℃ around the reference body t emperature, the slopes are similar, -0.031 and -0.033 respectively. To conclude, the temperature dependencies of ERG flash responses obtained *in vivo* correspond to those *ex vivo*, indicating that the whole body temperature manipulation method does not cause significant systematic error for the calibration of the temperature dependencies. Therefore, the retinal temperature estimation models should perform well inside the linear range of the determined features. However, when the heating temperature is high enough to cause substantial molecular damage, the ERG responses are expected to decay and temperature

determination becomes unreliable. Based on the experiments presented in this article and assuming that no significant difference exists between core body temperature and retinal temperature in our setup, the temperature estimation model should be applicable at least up to 42.5 ℃ (see Figs. 5 and 6).

In retinal heating, the transpupillary light is strongly absorbed by melanin pigments of the RPE, and heat conducts towards the neural retina. In the proposed temperature estimation method, the temperature-related information is retrieved from the a- and b-waves of ERG responses, originating mainly in the photoreceptor and bipolar cell layers in the distal retina. The RPE is located immediately behind the distal retina with negligible vasculature in or between, favoring the similarity of the temperatures in these two tissue layers. In retinal heating, the similarity of the temperatures in these tissues increases as a function of heating duration, as the heat dissipates towards the inner retina. In an experimental work with rabbits, no temperature differences could be observed between the subretinal space and the inner limiting membrane during one minute fundus heating with a 810 nm laser diode (Ibarra et al., 2004). We conclude that the ERG-based retinal temperature estimation method developed here is applicable for estimating the temperature of the distal retina, which is helpful when trying to avoid damage in the neural retina. In addition, in long heating treatments, the method can provide a good approximation of the temperature of the RPE layer.

4.2 Considerations for on-line temperature monitoring

The demonstrated method for mouse retinal and RPE temperature monitoring is applicable for heating treatment studies as well as for other basic research purposes where the retina undergoes non-damaging and lengthy increase in temperature. The method was calibrated using full-field ERG, but it can be applied for retrieving local retinal temperature estimates by directing the ERG stimulus light within the heated retinal area. Some stray light may end up outside the targeted area, but this light is expected to be negligible, especially with dim stimuli. Thus, it would not affect the ERG responses significantly. As the signal-to-noise ratio of the ERG response decreases with diminishing stimulus spot size, the temperature estimation method is most easily

utilized with large heated areas, and the application to small heated spots may require further development e.g. in signal processing approaches.

The demonstrated method can be implemented in the following manner. Before the beginning of the heating, ERG flash responses are recorded by stimulating the retinal area of interest at reference (normal) body temperature to determine the initial values of the chosen temperature dependent features. Thereafter, the same flashes are continuously applied with certain intervals to detect the changes in feature values and, thus, measure the temperature change compared to the initial temperature. This paper offers means for selecting the flash stimuli and the features to be extracted. After each bright flash response, approximately 20-second interval is needed for the recovery of photoresponse mechanisms. In a corresponding time period, at least five repetitions of dim flash responses can be recorded, providing higher accuracy (lower RMS error) and better temporal resolution for temperature estimation based on our results. Thus, these results recommend using dim flash responses for temperature monitoring. However, applying bright flash responses might be reasonable to supplement the temperature estimation with features extracted from the a-wave leading edge originating closer to the RPE.

The method presented in this paper is designed for the scotopic flash responses of the rod-dominant mouse retina. The dark-adapted state is easy to maintain with long enough interstimulus intervals, but attention must be paid when using transpupillary heating laser, the wavelength of which must be long enough to avoid light adaptation. Considering a corresponding temperature estimation method for clinical heating treatments of human cone-dominant retina, it would be appropriate to use light-adapted focal ERG with stimulus light directed inside the heated area, in the presence of background light. This would eliminate the requirement for dark environment and enable the usage of common wavelengths of lengthy heating treatments (e.g. 810 nm). With cone-driven ERG, the light adaptation level should be kept constant before and during laser irradiation in order not to confound the temperature determination.

5. ACKNOWLEDGEMENTS

This work was supported by the Academy of Finland (grant number 269747), Instrumentarium Science Foundation, and Tekes – the Finnish Funding Agency for Innovation (grant number 1575/31/2016).

6. REFERENCES

Baylor, D.A., Matthews, G., Yau, K.-W., 1983. Temperature effects on the membrane current of retinal rods of the toad. J. Physiol. 337, 723–734.

Connolly, B.P., Regillo, C.D., Eagle, R.C., Shields, C.L., Shields, J.A., Moran, H., 2003. The histopathologic effects of transpupillary thermotherapy in human eyes. Ophthalmology 110, 415–420. https://doi.org/10.1016/S0161-6420(02)01561-0

Donner, K., Hemilä, S., Koskelainen, A., 1988. Temperature-dependence of rod photoresponses from the aspartate-treated retina of the frog (Rana temporaria). Acta Physiol. Scand. 134, 535–541. https://doi.org/10.1111/j.1748-1716.1998.tb08528.x

Friedburg, C., Thomas, M.M., Lamb, T.D., 2001. Time course of the flash response of dark- and light- adapted human rod photoreceptors derived from the electroretinogram. J. Physiol. 534, 217–242. https://doi.org/10.1111/j.1469-7793.2001.t01-1-00217.x

Ibarra, M.S., Hsu, J., Mirza, N., Wu, I.H., Ying, G.S., Mainster, M.A., Tolentino, M.J., 2004. Retinal temperature increase during transpupillary thermotherapy: Effects of pigmentation, subretinal blood, and choroidal blood flow. Investig. Ophthalmol. Vis. Sci. 45, 3678–3682. https://doi.org/10.1167/iovs.04-0436

Kong, J., Gouras, P., 2003. The effect of body temperature on the murine electroretinogram. Doc. Ophthalmol. 106, 239–242.

Koskelainen, A., Ala-Laurila, P., Fyhrquist, N., Donner, K., 2000. Measurement of thermal contribution to photoreceptor sensitivity. Nature 403, 220–223. https://doi.org/10.1038/35003242

518 Koss, M.J., Beger, I., Koch, F.H., 2012. Subthreshold diode laser micropulse
519 photocoagulation versus intravitreal injections of bevacizumab in the treatment of
520 central serous chorioretinopathy. Eye 26, 307–314.
521 https://doi.org/10.1038/eye.2011.282

522 Lamb, T.D., 1984. Effects of temperature changes on toad rod photocurrents. J.
523 Physiol. 346, 557–578.

524 Lavinsky, D., Wang, J., Huie, P., Dalal, R., Lee, S.J., Lee, D.Y., Palanker, D., 2016.
525 Nondamaging retinal laser therapy: Rationale and applications to the macula.
526 Investig. Ophthalmol. Vis. Sci. 57, 2488–2500. https://doi.org/10.1167/iovs.15-
527 18981

528 Luttrull, J.K., Chang, D.B., Margolis, B.W.L., Dorin, G., Luttrull, D.K., 2015. Laser
529 resensitization of medically unresponsive neovascular age-related macular
530 degeneration. Retina 35, 1184–1194.
531 https://doi.org/10.1097/IAE.0000000000000458

532 Mizota, A., Adachi-Usami, E., 2002. Effect of body temperature on electroretinogram of
533 mice. Invest. Ophthalmol. Vis. Sci. 43, 3754–3757.

534 Nymark, S., Heikkinen, H., Haldin, C., Donner, K., Koskelainen, A., 2005. Light
535 responses and light adaptation in rat retinal rods at different temperatures. J.
536 Physiol. 567, 923–938. https://doi.org/10.1113/jphysiol.2005.090662

537 Parver, L.M., 1991. Temperature modulating action of choroidal blood flow. Eye 5, 181–
538 185.

539 Pitkänen, M., Kaikkonen, O., Koskelainen, A., 2017. A novel method for mouse retinal
540 temperature determination based on ERG photoresponses. Ann. Biomed. Eng. 45,
541 2360–2372. https://doi.org/10.1007/s10439-017-1872-y

542 Ridder, W.H., Nusinowitz, S., Heckenlively, J.R., 2002. Causes of cataract development
543 in anesthetized mice. Exp. Eye Res. 75, 365–370. https://doi.org/10.1016/S0014-
544 4835(02)92007-5

545 Robinson, D.W., Ratto, G.M., Lagnado, L., McNaughton, P.A., 1993. Temperature

546 dependence of the light response in rat rods. J. Physiol. 462, 465–481.

547 Scholz, P., Altay, L., Fauser, S., 2017. A review of subthreshold micropulse laser for
548 treatment of macular disorders. Adv. Ther. 34, 1528–1555.
549 https://doi.org/10.1007/s12325-017-0559-y

550 Sivaprasad, S., Elagouz, M., Mchugh, D., Shona, O., Dorin, G., 2010. Micropulsed
551 diode laser therapy: evolution and clinical applications. Surv. Ophthalmol. 55, 516–
552 530. https://doi.org/10.1016/j.survophthal.2010.02.005

553 Söderberg, A.-C., Algvere, P. V, Hengstler, J.C., Söderberg, P., Seregard, S., Kvanta,
554 A., 2012. Combination therapy with low-dose transpupillary thermotherapy and
555 intravitreal ranibizumab for neovascular age-related macular degeneration: a 24-
556 month prospective randomised clinical study. Br. J. Ophthalmol. 96, 714–8.
557 https://doi.org/10.1136/bjophthalmol-2011-300721

558 Sramek, C., Mackanos, M., Spitler, R., Leung, L.S., Nomoto, H., Contag, C.H.,
559 Palanker, D., 2011. Non-damaging retinal phototherapy: Dynamic range of heat
560 shock protein expression. Investig. Ophthalmol. Vis. Sci. 52, 1780–1787.
561 https://doi.org/10.1167/iovs.10-5917

562 St. George, R.C.C., 1952. The interplay of light and heat in bleaching rhodopsin. J. Gen.
563 Physiol. 35, 495–517.

564 Stiles, W.S., 1948. The physical interpretation of the spectral sensitivity curve of the
565 eye, in: Transactions of the Optical Convention of the Worshipful Company of
566 Spectacle Makers. Spectacle Makers' Company London, pp. 97–107.

567 Tode, J., Richert, E., Koinzer, S., Klettner, A., Der, C. Von, Brinkmann, R., Lucius, R.,
568 Roider, J., 2018. Thermal stimulation of the retina reduces bruch's membrane
569 thickness in age related macular degeneration mouse models. Transl Vis Sci
570 Technol 7, 2.

571 Vinberg, F., Koskelainen, A., 2010. Calcium sets the physiological value of the dominant
572 time constant of saturated mouse rod photoresponse recovery. PLoS One 5,
573 e13025. https://doi.org/10.1371/journal.pone.0013025

574

575 **Figure 1.** The mouse was placed in a tilted bath with water up to ear-level. Water was
576 circulated in the bath to control the body temperature of the mouse.

577 **Figure 2.** A) *In vivo* ERG responses recorded from mouse cornea. Each trace
578 represents a single response, low-pass filtered with f_c = 1 kHz. Stimulus strength was
579 modified by changing flash length (0.15 µs – 0.5 ms). B) Selecting stimulus strengths
580 based on operation range. B-wave reference amplitude, 'b-ref-amp', was determined
581 from a response with a small emerging a-wave (black dashed lines). At this level, b-
582 wave amplitude shows plateau-like behavior as a function of flash strength. Dim flash
583 strengths were selected to give rise to 20, 30 and 40% amplitudes of b-ref-amp (red
584 dashed lines). The flash length used as a bright flash was approximately 1000 times
585 longer than the one used for the 20% response (purple dashed lines) C) ERG
586 responses to the same bright flash strength recorded at two different temperatures. The
587 features that were extracted from the leading edge of the a-wave have been visualized.
588 The responses are single filtered recordings (FIR, n = 50, f_c = 100 Hz) that have been
589 normalized to the a-wave amplitude. D) ERG responses to the same dim flashes
590 recorded at two different temperatures. The features representing the dim flash
591 responses are listed in the figure. The responses are single filtered recordings (FIR, n =
592 400, fc = 30 Hz) that have been normalized to the b-wave amplitude.

593 **Figure 3.** The effect of dim flash strength on temperature dependence of b-wave time-
594 to-peak. Each data point represents b-wave time-to-peak defined from 5 – 20 averaged
595 responses and normalized with corresponding value at reference temperature according
596 to $(b100_{temp} - b100_{ref}) \cdot b100_{ref}^{-1}$. Responses have different amplitudes compared to b-
597 wave reference amplitude: 20% (black circle), 30% (red diamond), and 40% (blue
598 triangle). The plot includes those experiments from the training data set, in which all
599 three response types were recorded.

600 **Table 1.** [a] Features #1–12 are determined from single bright flash responses, #13–33
601 are based on 5-20 averaged dim flash responses. [b] Slopes of linear fittings to the
602 training data (as illustrated in Figure 4) and root mean square deviations (residuals)

603 between the fit and the data. RMSD has the same unit, relative feature value, as the y-
604 axes in Fig. 4. Correspondingly, the unit of the slope is relative feature value per degree
605 of Celsius. [c] Low dispersion of feature values around the linear fitting (i.e. small
606 residuals) and a high temperature dependence are beneficial properties for a feature.
607 RMSD/|Slope| reflects the relationship of these properties, low value being desirable.

#[a]	Feature	Response type	Abbr.	Slope[b]	RMSD[c]	RMSD/ |Slope|[d]
1	Time to 10 % of the peak	bright flash, a-wave	a10	-0,032	0,281	8,73
2	Time to 20 % of the peak	bright flash, a-wave	a20	-0,030	0,180	5,91
3	Time to 30 % of the peak	bright flash, a-wave	a30	-0,029	0,133	4,59
4	Time to 40 % of the peak	bright flash, a-wave	a40	-0,030	0,095	3,22
5	Time to 50 % of the peak	bright flash, a-wave	a50	-0,030	0,073	2,43
6	Time to 60 % of the peak	bright flash, a-wave	a60	-0,030	0,060	2,00
7	Time to 70 % of the peak	bright flash, a-wave	a70	-0,030	0,046	1,53
8	Time to 80 % of the peak	bright flash, a-wave	a80	-0,031	0,037	1,20
9	Time to 90 % of the peak	bright flash, a-wave	a90	-0,033	0,033	1,01
10	Time to peak	bright flash, a-wave	a100	-0,034	0,028	0,82
11	Time to inflection point	bright flash, a-wave	aip	-0,019	0,022	1,14
12	Stretch	bright flash, a-wave	ast	-0.024	0.033	1.39
13	Time to 10 % of the peak	dim flash, b-wave leading edge	b10L	-0,025	0,045	1,78
14	Time to 20 % of the peak	dim flash, b-wave leading edge	b20L	-0,027	0,028	1,05
15	Time to 30 % of the peak	dim flash, b-wave leading edge	b30L	-0,027	0,022	0,82
16	Time to 40 % of the peak	dim flash, b-wave leading edge	b40L	-0,027	0,020	0,72
17	Time to 50 % of the peak	dim flash, b-wave leading edge	b50L	-0,028	0,018	0,67
18	Time to 60 % of the peak	dim flash, b-wave leading edge	b60L	-0,028	0,018	0,64
19	Time to 70 % of the peak	dim flash, b-wave leading edge	b70L	-0,028	0,018	0,63
20	Time to 80 % of the peak	dim flash, b-wave leading edge	b80L	-0,028	0,018	0,63
21	Time to 90 % of the peak	dim flash, b-wave leading edge	b90L	-0,029	0,018	0,64
22	Time to peak	dim flash, b-wave	b100	-0,036	0,023	0,65
23	Time to 90 % of the peak	dim flash, b-wave trailing edge	b90T	-0,032	0,025	0,76
24	Time to 80 % of the peak	dim flash, b-wave trailing edge	b80T	-0,033	0,025	0,78
25	Time to 70 % of the peak	dim flash, b-wave trailing edge	b70T	-0,032	0,026	0,82

26	Time to 60 % of the peak	dim flash, b-wave trailing edge	b60T	-0,032	0,029	0,91
27	Time to 50 % of the peak	dim flash, b-wave trailing edge	b50T	-0,032	0,030	0,96
28	Time to 40 % of the peak	dim flash, b-wave trailing edge	b40T	-0,032	0,032	1,00
29	Time to 30 % of the peak	dim flash, b-wave trailing edge	b30T	-0,032	0,037	1,18
30	Time to 20 % of the peak	dim flash, b-wave trailing edge	b20T	-0,031	0,048	1,56
31	Time to 10 % of the peak	dim flash, b-wave trailing edge	b10T	-0,031	0,082	2,69
32	Integration time	dim flash, b-wave	bit	-0,034	0,058	1,68
33	Stretch	dim flash, b-wave	bst	-0.031	0.025	0.79

Figure 4. Temperature-dependencies of example features in training dataset (n = 14 mice). Feature values have been normalized with corresponding feature values recorded at reference body temperature according to equation $(Y_{temp} - Y_{ref}) \cdot Y_{ref}^{-1}$. The temperature is denoted as the difference compared to the reference temperature. A linear least squares fit is illustrated in each plot, the equation of the fit given above the x-axis. A) Time-to-peak of bright flash response a-wave, B) time to inflection point of the bright flash response a-wave, C) time-to-70% of the peak of dim flash response leading edge, D) time-to-peak of dim flash response b-wave, E) integration time of dim flash response b-wave, F) stretch-feature of the b-wave.

Figure 5. Model development and validation for bright flash responses. A) Temperature determination errors averaged over cross validations and expressed as RMS values for each linear regression model constructed of a single feature. B) Lowest BIC values of models containing a certain number of features. C) Relationship between estimated and measured temperatures, when applying the constructed model on new data. D) Histogram of temperature determination errors ($T_{estimated}$ - $T_{measured}$) illustrating error magnitudes and the shape of the error distribution.

Figure 6. Model development and validation for dim flash responses. A) Temperature determination errors averaged over cross validations and expressed as RMS values for each linear regression model constructed of a single feature. B) Lowest BIC values of models containing a certain number of features. C) Relationship between estimated and measured temperatures, when applying the constructed model on new data. D)

Histogram of temperature determination errors ($T_{estimated}$ - $T_{measured}$) illustrating error magnitudes and the shape of the error distribution.

Figure 7. Examination of stimulus intervals for continuous temperature estimation. A) Sequences of four dim flash responses were recorded with stimulus intervals 0.5-0.8 s (black squares), 1.0-1.3 s (red circles), 2.0-2.3 s (blue triangles), 3.0-3.3 s (green diamonds), and 4.0-4.3 s (purple stars). Between each sequence, the retina was dark adapted for at least 10 seconds. The time-to-peak of the b-wave was determined from the responses and normalized according to the time-to-peak of the first response in the sequence. Each stimulus interval category was tested with n = 3 - 6 mice and the number of repetitions for each stimulus interval was 10 – 46. The results are illustrated as mean ± SEM. B) After a single bright flash, series of very dim flash responses (amplitude ~10% of b-wave reference amplitude) were recorded, the first one 3 seconds after the bright flash and then with 4 s interval. The last responses of the series were recorded with 10 s interval. Very dim flashes were applied here to minimize the lengthening of the light adapted period due to dim flash series. The recording protocol was repeated 3-5 times with n = 3 mice. An exponential fit was performed to each time-to-peak series, and the values were normalized with the plateau level obtained from the fit. The data is presented as mean ± SEM. An exponential shown in the figure (red trace) is obtained by fitting to the averaged data.

Figure S1. A-wave time-to-peak shows similar temperature-dependence when determined from *in vivo* (black circles) and *ex vivo* (blue stars) photoresponses in the temperature range of -2.0 … +4.5 ℃. At higher temperatures, nonlinear behavior emerges to *ex vivo* time-to-peak. Temperature dependence slope determined by least squares linear fit was -0.033 for *in vivo* time-to-peak (black dashed trace) and -0.031 for *ex vivo* time-to-peak (red dashed trace) in the range of -2.0 … +4.5 ℃. The corresponding slope fitted to all *ex vivo* data is -0.023 (blue dashed trace).

APPENDIX

The baseline of each response was set to zero by generating an autoregressive model of order 5000 based on the ERG signal preceding the stimulus. With the model, the signal baseline behavior after the stimulus was estimated and subtracted from the response. This baseline correction method diminishes periodical artefacts caused e.g. by mouse breathing movements.

Responses were low pass FIR-filtered using the following cutoff frequencies, f_c, and orders, n: features #1-10: f_c = 100, n = 50; #11-12: f_c = 40, n = 300; #13-21 and #33: f_c = 20, n = 600; #23-32: f_c = 30, n = 400; and #22: no filtering. The level of filtering affects the slope of temperature dependence. Therefore, filter parameters were selected according to our previous publication with *ex vivo* ERG (Pitkänen et al., 2017) to enable comparison of temperature dependencies between these two modalities. However, it should be noted that the number of averaged responses differs compared to our previous work, and thus, the dispersion of feature values cannot be directly compared.

The peak of the a-wave was located by proceeding through the leading edge of the bright flash response and finding the time point t_{max} where the subtraction of response values $V(t + 1ms) - V(t - 1ms)$ changed sign. The location of the peak was slightly corrected by fitting a quadratic polynomial between $[t_{max} - 2ms, t_{max} + 2ms]$ and the minimum of this fit defined the time-to-peak, t_{a-peak}, and the amplitude of the a-wave, $a - peak$. Thereafter, the time-to-X% of a-wave peak could be defined as the time point t_{a-X} at which the comparison $V(t) < X\% \cdot a - peak$ became true. The inflection point was determined as the local minimum of the derivative of a cubic polynomial fitted to the leading edge of the a-wave.

The peak of the b-wave was located by fitting a quadratic polynomial around the global maximum of the dim flash response $[t_{max} - 30ms, t_{max} + 30ms]$. The location of the peak was slightly corrected by repeating the fitting around the peak obtained from the first fit. The maximum of the second fit defined the time-to-peak, t_{b-peak}, and the amplitude of the b-wave, $b - peak$. The time-to-X% features of the b-wave leading edge (t_{bl-X}) and trailing edge (t_{bt-X}) were determined as time points where the comparisons $V(t) > X\% \cdot b - peak,\ t > 0$ and $V(t) < X\% \cdot b - peak, t > t_{b-peak}$ became true,

687 respectively. The integration time was determined by calculating the integral of the
688 response by trapezoidal method from $t = t_{bl-40}$ until $t = t_{bt-40}$. The integral was
689 divided by the amplitude $b - peak$.

690 The stretch feature measures the amount of stretching or compressing needed for the
691 response recorded at elevated or lowered temperature to coincide with the reference
692 response. The re-scaling of the time axis was obtained by calculating linearly
693 interpolated values of each response at new time points obtained by multiplying the
694 original time axis with a factor between 0.75 and 1.15. The factor leading to the lowest
695 sum of squared errors compared to the reference response defined the feature value.
696 For the a-wave, the responses were at first divided by the amplitude $a - peak$ and the
697 sum of squared errors was calculated between time points $[10ms, t_{a-peak}]$. For the b-
698 wave, normalizing responses was found unnecessary and the sum of squared errors
699 was calculated between $[0ms, 300ms]$.

- Mouse corneal ERG recording provides means for monitoring the temperature of the distal retina and the RPE.

- Five scotopic dim flash responses enabled the estimation of distal retina temperature with an RMS error of 0.68 ℃.

- Both bright flash response a-wave and dim flash response b-wave are applicable for temperature estimation, but b-waves provide better accuracy with higher temporal resolution.

- The accuracy of the developed retinal temperature estimation method enables the control of the heating power in non-damaging retinal heating treatments.

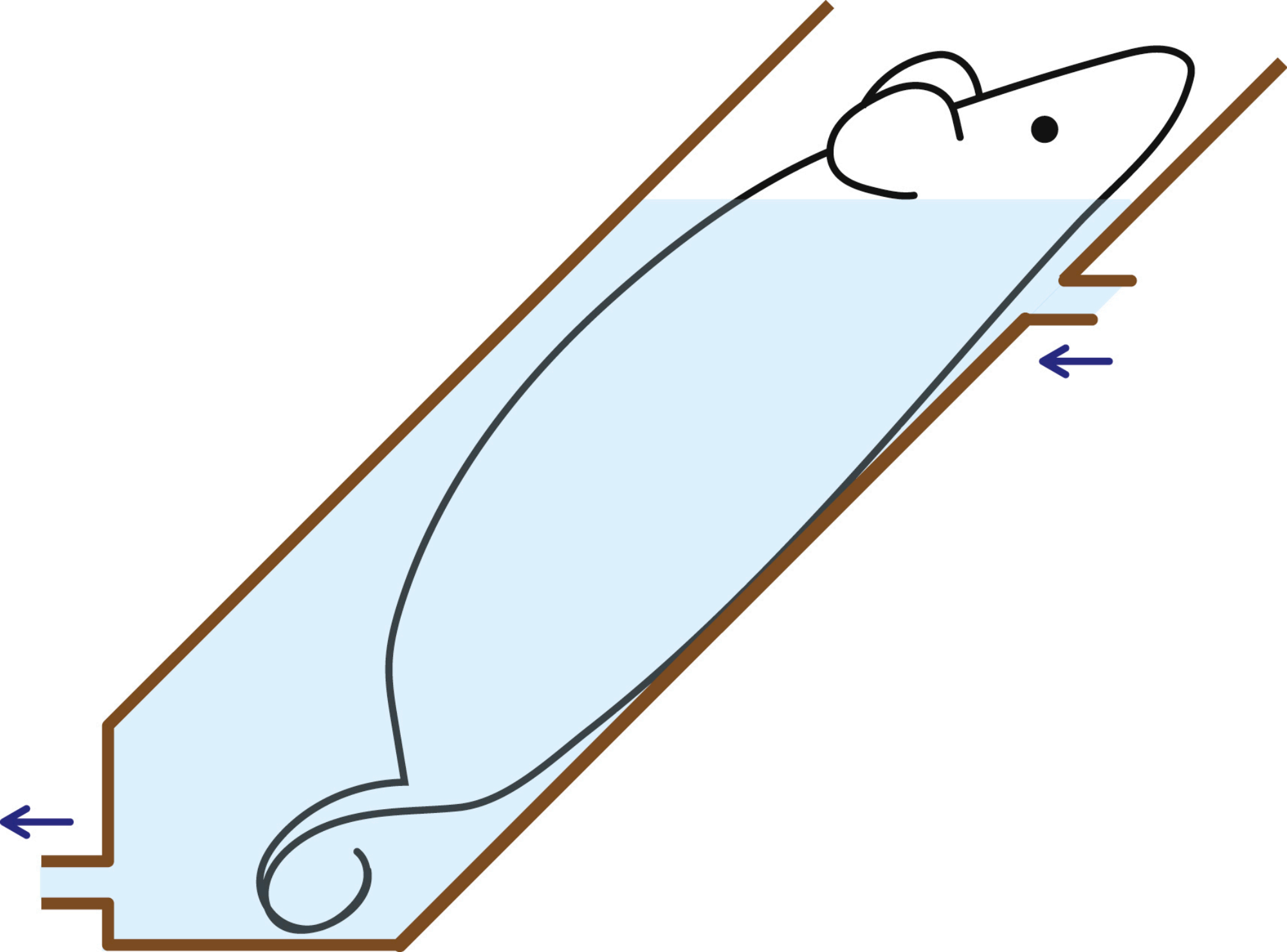

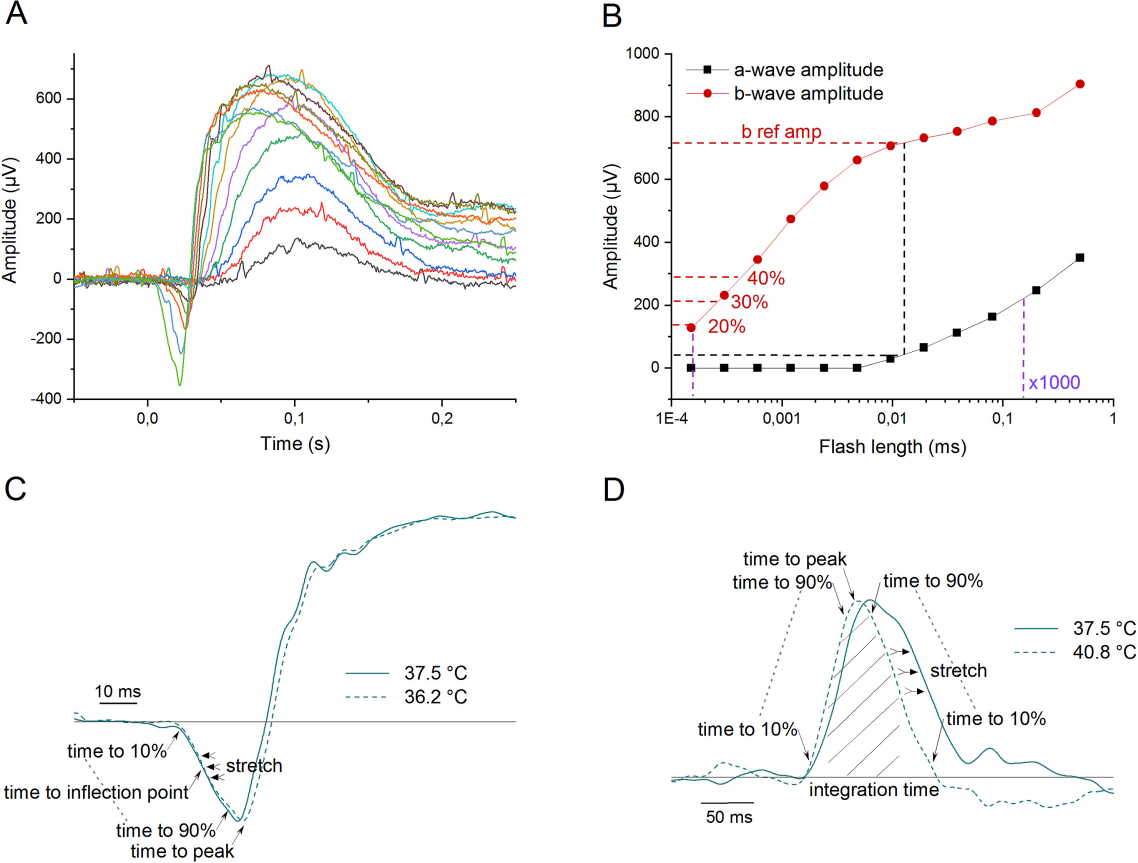
A
Amplitude (µV)
600
400
200
0
-200
-400
0,0
0,1
0,2
Time (s)
B
a-wave amplitude
b-wave amplitude
b ref amp
40%
30%
20%
x1000
Amplitude (µV)
1000
800
600
400
200
0
1E-4
0,001
0,01
0,1
1
Flash length (ms)
C
37.5 °C
36.2 °C
10 ms
time to 10%
stretch
time to inflection point
time to 90%
time to peak
D
time to peak
time to 90%
time to 90%
37.5 °C
40.8 °C
stretch
time to 10%
time to 10%
integration time
50 ms

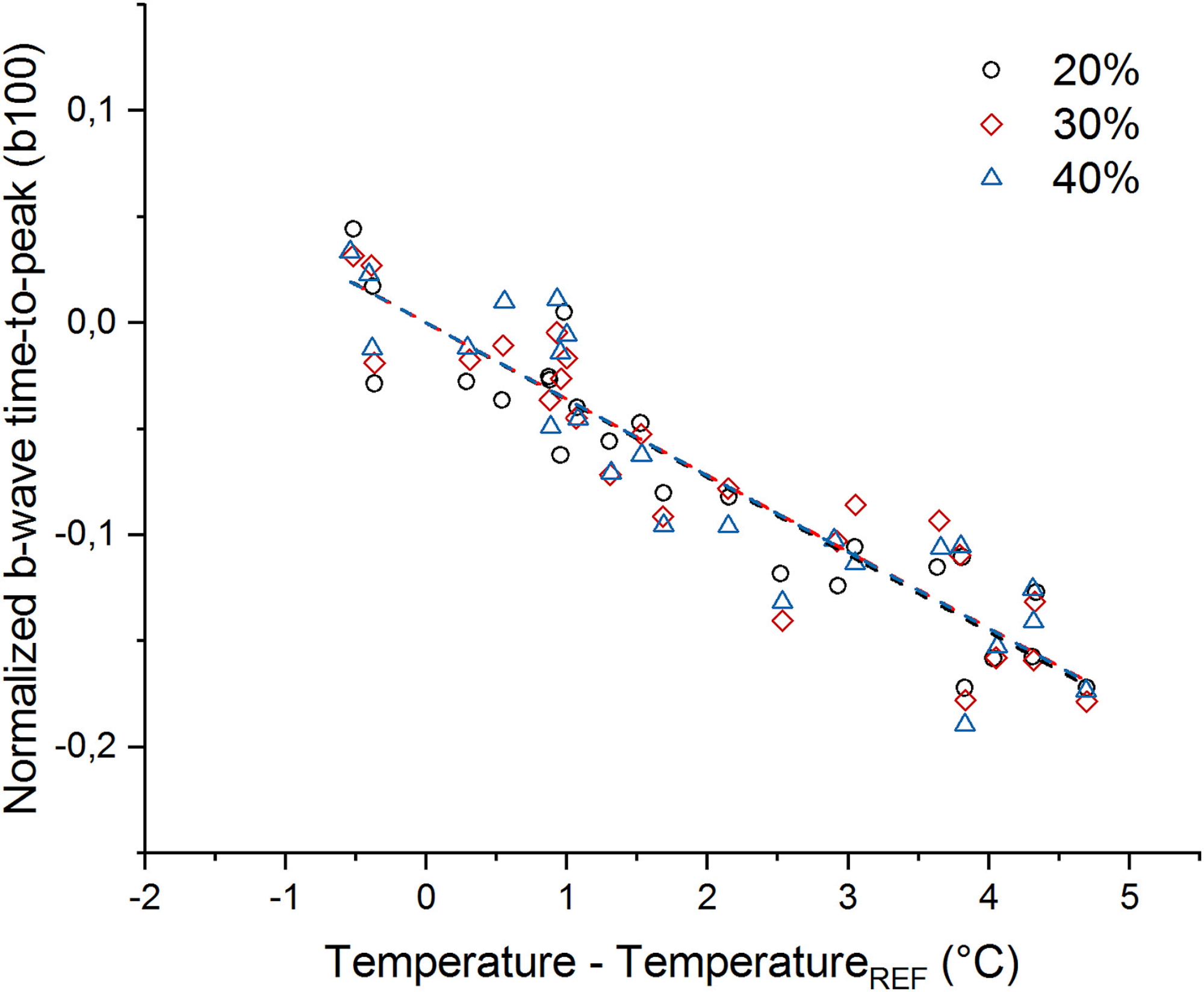
20%
30%
40%
Normalized b-wave time-to-peak (b100)
0,1
0,0
-0,1
-0,2
-2
-1
0
1
2
3
4
5
Temperature - Temperature$_{REF}$ (°C)

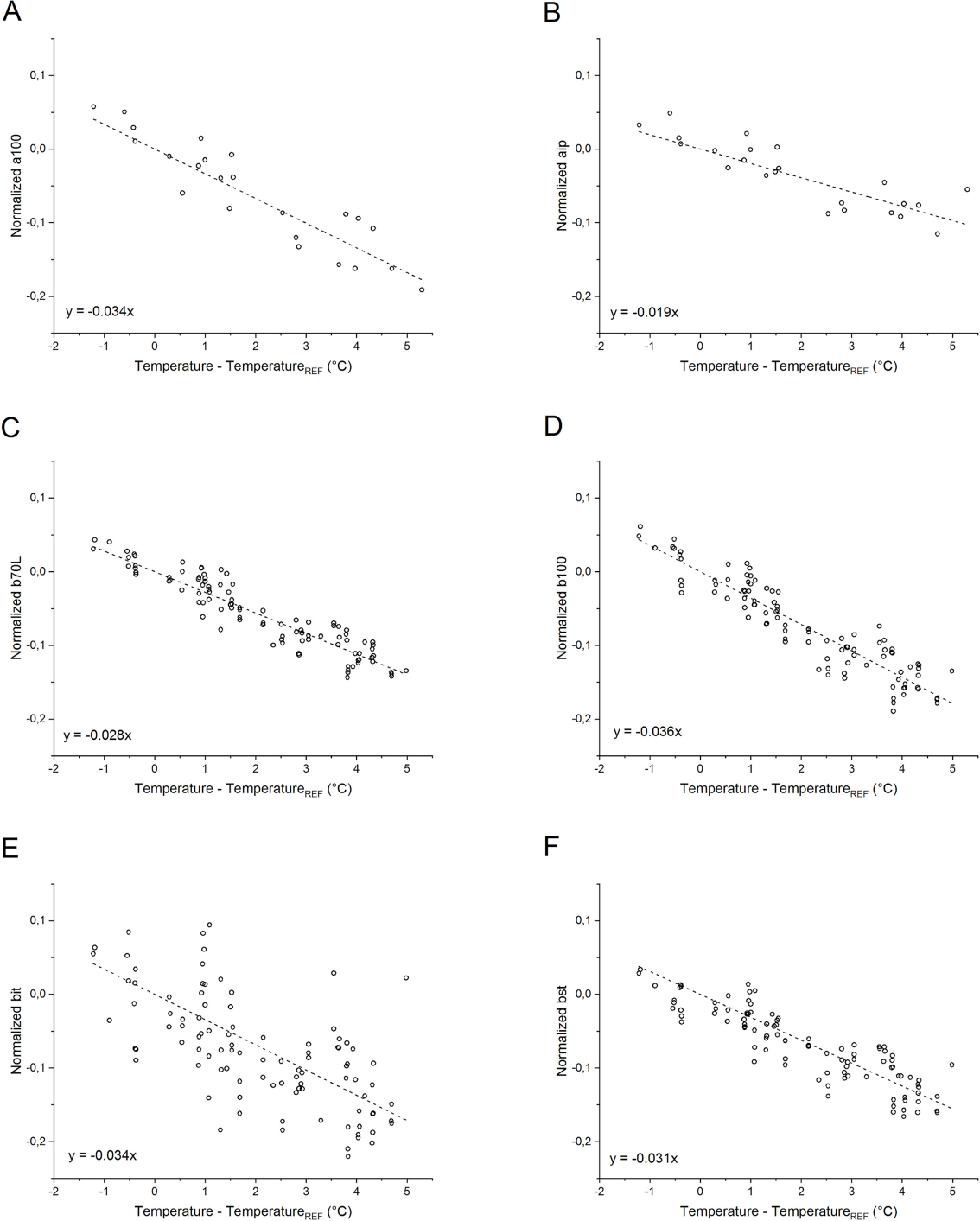
A
Normalized a100
y = -0.034x
Temperature - Temperature$_{REF}$ (°C)
B
Normalized aip
y = -0.019x
Temperature - Temperature$_{REF}$ (°C)
C
Normalized b70L
y = -0.028x
Temperature - Temperature$_{REF}$ (°C)
D
Normalized b100
y = -0.036x
Temperature - Temperature$_{REF}$ (°C)
E
Normalized bit
y = -0.034x
Temperature - Temperature$_{REF}$ (°C)
F
Normalized bst
y = -0.031x
Temperature - Temperature$_{REF}$ (°C)

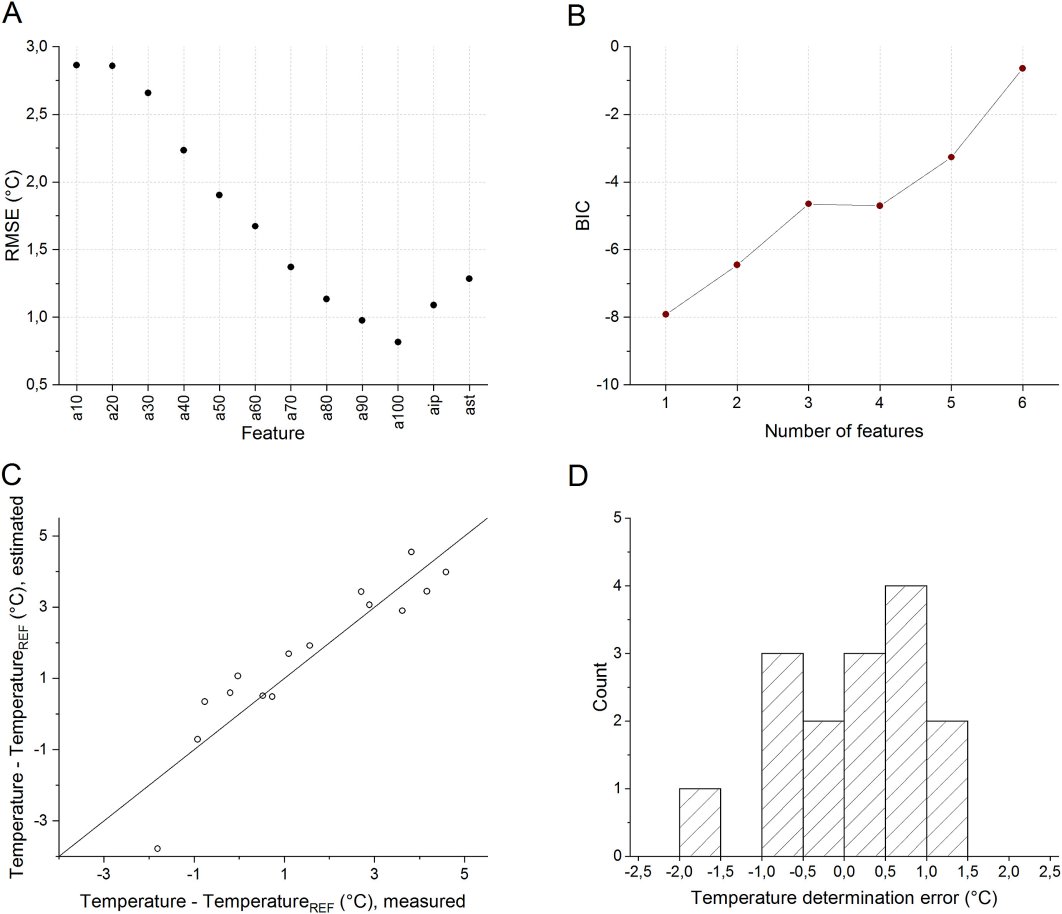
A
RMSE (°C)
3,0
2,5
2,0
1,5
1,0
0,5
a10
a20
a30
a40
a50
a60
a70
a80
a90
a100
aip
ast
Feature
B
BIC
0
-2
-4
-6
-8
-10
1
2
3
4
5
6
Number of features
C
Temperature - Temperature$_{REF}$ (°C), estimated
5
3
1
-1
-3
-3
-1
1
3
5
Temperature - Temperature$_{REF}$ (°C), measured
D
Count
5
4
3
2
1
0
-2,5
-2,0
-1,5
-1,0
-0,5
0,0
0,5
1,0
1,5
2,0
2,5
Temperature determination error (°C)

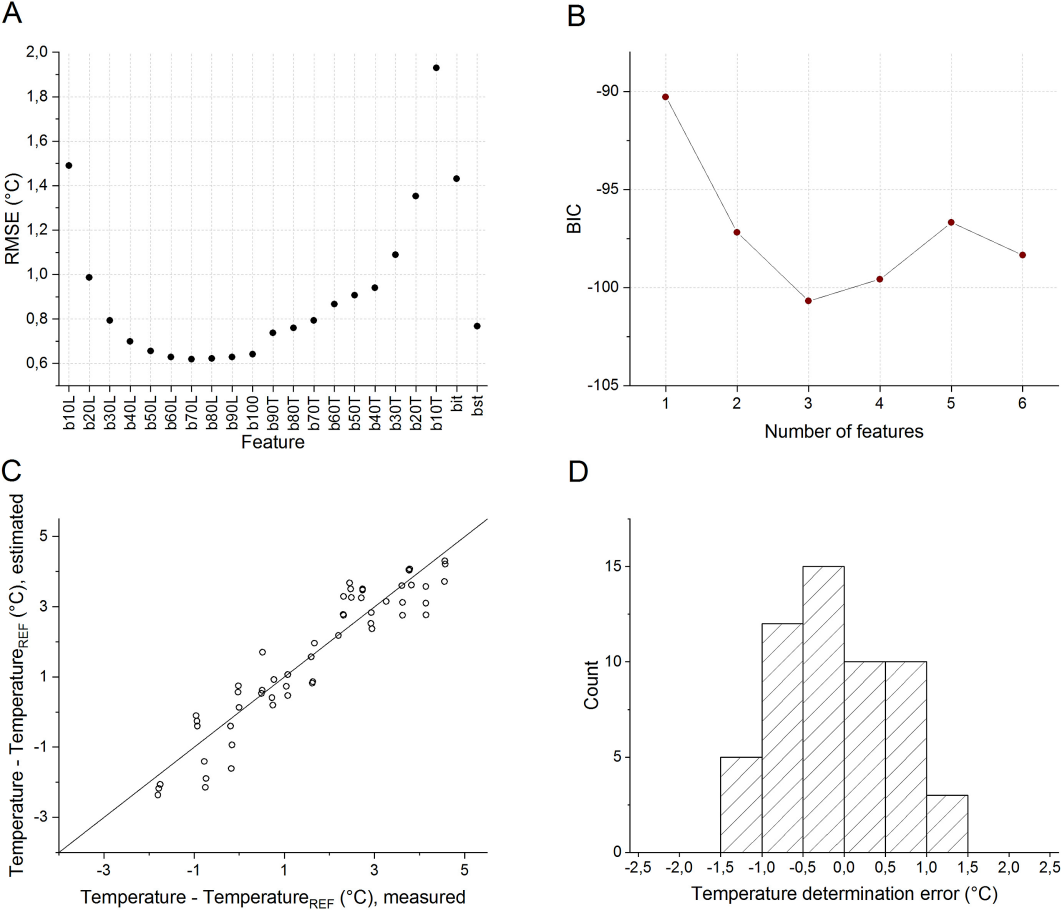
A
RMSE (°C)
2,0
1,8
1,6
1,4
1,2
1,0
0,8
0,6
b10L
b20L
b30L
b40L
b50L
b60L
b70L
b80L
b90L
b100
b90T
b80T
b70T
b60T
b50T
b40T
b30T
b20T
b10T
bit
bst
Feature
B
BIC
-90
-95
-100
-105
1
2
3
4
5
6
Number of features
C
Temperature - Temperature$_{REF}$ (°C), estimated
5
3
1
-1
-3
-3
-1
1
3
5
Temperature - Temperature$_{REF}$ (°C), measured
D
Count
15
10
5
0
-2,5
-2,0
-1,5
-1,0
-0,5
0,0
0,5
1,0
1,5
2,0
2,5
Temperature determination error (°C)

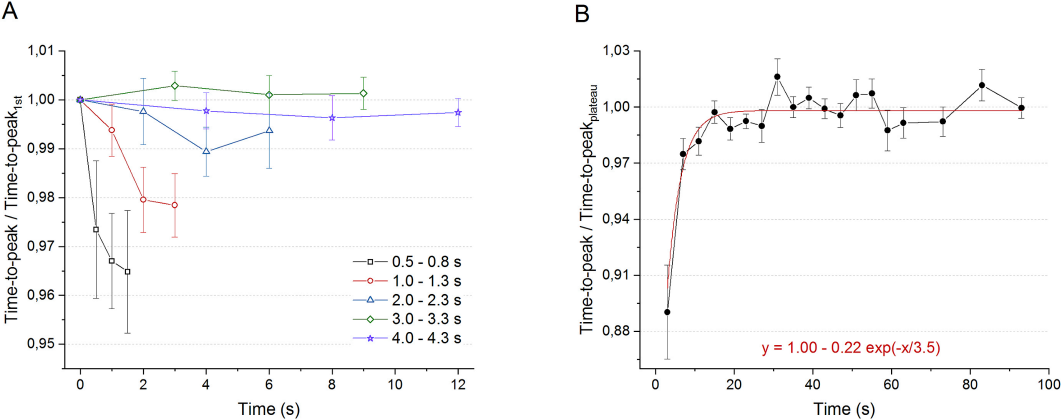
A
Time-to-peak / Time-to-peak1st
1,01
1,00
0,99
0,98
0,97
0,96
0,95
0
2
4
6
8
10
12
Time (s)
0.5 - 0.8 s
1.0 - 1.3 s
2.0 - 2.3 s
3.0 - 3.3 s
4.0 - 4.3 s
B
Time-to-peak / Time-to-peakplateau
1,03
1,00
0,97
0,94
0,91
0,88
0
20
40
60
80
100
Time (s)
y = 1.00 - 0.22 exp(-x/3.5)